Journal of Ethnopharmacology 319 (2024) 117164

Contents lists available at ScienceDirect

Journal of Ethnopharmacology

journal homepage: www.elsevier.com/locate/jethpharm

Ruyong formula improves thymus function of CUMS-stimulated breast cancer mice

Bingqian He [a,1], Wenqin Guo [b,c,1], Rongzhen Shi [b,d,1], Robert D. Hoffman [e], Qihan Luo [b], Yuan-Jia Hu [f,**], Jianli Gao [b,*]

[a] Academy of Chinese Medical Science, Zhejiang Chinese Medical University, Hangzhou, 310053, China
[b] School of Pharmaceutical Sciences, Zhejiang Chinese Medical University, Hangzhou, 310053, China
[c] School of Basic Medical Sciences, Zhejiang Chinese Medical University, Hangzhou, 310053, China
[d] Tangqi Branch of Traditional Chinese Medicine Hospital of Linping District, Hangzhou, Zhejiang, 311106, China
[e] Yo San University of Traditional Chinese Medicine, Los Angeles, CA, 90066, USA
[f] State Key Laboratory of Quality Research in Chinese Medicine, University of Macau, Macao, 999078, China

ARTICLE INFO

Keywords:
Ruyong formula
Breast cancer
Epithelial mesenchymal transition
CUMS
Thymus function
JAK2/STAT3/PI3K pathway

ABSTRACT

Ethnopharmacological relevance: Ruyong Formula (RYF) is a famous Chinese herbal formula composed of 10 traditional Chinese herbs. It has been used as a therapeutic agent for breast cancer patients with depressive symptoms in China. However, its underlying pharmacological mechanism remains unclear.

Aim of the study: This study aimed to explore the mechanism of RYF on the changes of thymus immune function in breast cancer body under mood disorders such as depression/anxiety.

Materials and methods: The chronic unpredictable mild stress (CUMS) was used to stimulate 4T1 breast cancer mice. The behavioral changes, 5-hydroxytryptamine (5-HT) level in brain, cytokeratin 5 (CK5) and 8 (CK8) expression in thymus, the proportion of T cell subsets, the thymic output, phenotypic changes of thymus epithelial cells (TECs), the expression levels of immune-related factors and downstream proteins of TSLP were analyzed after RYF treatment.

Results: In CUMS stimulated group, the level of 5-HT in brain was significantly increased after RYF treatment. The output function of the thymus was improved, and the number of TECs in the medulla ($CK5^+$), the proportion of $CD3^+CD4^-CD8^-$ (Double negative) and $CD3^+CD4^+CD8^+$ (Double positive) T cells were all increased. The mRNA level of TSLP in mouse thymus was significantly decreased, but increased for IL-7. The protein levels of TSLP and Vimentin were decreased, but increased for p-STAT3, p-JAK2, E-cadherin, and p-PI3K p55 *in vivo*. *In vitro* study was showed the levels of Snail 1, Zeb 1 and Smad increased significantly in TGF-β1 group, and RYF could reverse their expression.

Conclusions: RYF could restore the structure and function of the thymus in depressed breast cancer mice by reversing the phenotypic changes of TECs and activating the JAK2/STAT3/PI3K pathway.

1. Introduction

The human immune system is closely related to the central nervous system. As an important central immune organ, the thymus plays an important role in maintaining the normal immune function of the body (Alvarez-Mon et al., 2020, 2021; Boorman et al., 2016; Yu et al., 2022). Breast cancer is one of the high-incidence diseases of young and middle-aged women, and its incidence is increasing year by year. The immune function can be impacted by the emotional disorders and stress events, and changes in immune function may also become the cause of depression (Ma et al., 2021). Although the etiology of breast cancer has not been fully elucidated, previous studies have shown that depression and other negative emotions are closely related to the occurrence, development and prognosis of breast cancer (Borgi et al., 2020; Hajj et al., 2021; Lee et al., 2021; Lopes et al., 2022).

* Corresponding author.
** Corresponding author.
E-mail addresses: bingqianhe@126.com (B. He), gwqjxnc@126.com (W. Guo), 1152355821@qq.com (R. Shi), robmix3@gmail.com (R.D. Hoffman), 461289566@qq.com (Q. Luo), yuanjiahu@umac.mo (Y.-J. Hu), jianligao@zcmu.edu.cn (J. Gao).
[1] Bingqian He, Wenqin Guo and Rongzhen Shi contributed equally to this work.

https://doi.org/10.1016/j.jep.2023.117164
Received 30 May 2023; Received in revised form 20 August 2023; Accepted 8 September 2023
Available online 16 September 2023

Abbreviations

Abbreviations	*Full description*
RYF	Ruyong Formula
CUMS	chronic unpredictable mild stress
5-HT	5-hydroxytryptamine
CK5	cytokeratin 5
CK8	cytokeratin 8
TSLP	Thymic stromal lymphopoietin
TECs	thymus epithelial cells
IL-5	Interleukin-5
IL-6	Interleukin-6
IL-7	Interleukin-7
IL-10	Interleukin-10
IL-12	Interleukin-12
IL-1α	Interleukin-1α
STAT3	signal transducers and activators of transcription 3
p-STAT3	phospho-signal transducers and activators of transcription 3
JAK2	janus kinase 2
p-JAK2	phospho-janus kinase 2
PI3K	phosphoinositol 3 kinase
p-PI3K	phospho-phosphoinositol 3 kinase
TGF-β1	transforming growth factor-β1
EMT	epithelial-mesenchymal transition
HPLC	high-performance liquid chromatography
CTX	cyclophosphamide
OFT	open field test
FST	forced swim test
ELISA	enzyme-linked immunosorbent assay
H&E	hematoxylin and eosin
DMSO	dimethyl sulfoxide
iTEC	immortalized thymus epithelial cells
CD3	cluster of differentiation 3
CD4	cluster of differentiation 4
CD8	cluster of differentiation 8
TRECs	T cell receptor rearrangement excision circles
TNF-α	tumor necrosis factor-α
TSLP	thymic stromal lymphopoietin

Ruyong Formula (RYF) has been used for hundreds of years in China, with the earliest description being recorded in 1481 in "dan xi xin fa" (recording clinical experiences and prescriptions of Zhu Danxi, a famous doctor of Yuan Dynasty in China) (He et al., 2021; Zhu ZH, 2005). It has been shown to be effective against breast cancer in clinical studies (Huang et al., 2013; Liu et al., 2019). Furthermore, the quercetin and kaempferol in *Paeoniae Radix Alba* have obvious anti-anxiety and anti-tumor effects; paeoniflorin in *Radix Bupleuri* can improve depression and anxiety in experimental mice (Harrath et al., 2021; Tang et al., 2021; S. Zhang et al., 2021). Moreover, for improving the therapeutic efficacy, we established the empirical prescription formula, RYF, and modifying the classical SQFZ and SQDBT decoction (Huang et al., 2013; Liu et al., 2019). Ten crude herbs (shown in Table 1) constitute RYF. They improve the overall conditions of breast cancer patients, especially enhancing the immunity (Bao et al., 2014; Y. Wu et al., 1998; Xie et al., 2017). Our previous experimental studies showed that the thymic epithelial tissue of mice in the breast cancer model group was atrophied. *Astmgali Radix*, *Angelicae sinensis Radix*, etc. can enhance thymic function after administration, but the specific mechanism is still unclear, and there are few related studies, so it has certain research significance.

Epithelialization of the thymus epithelial cells (TEC) is a critical step in breast cancer. Epithelial-mesenchymal transition (EMT), has been increasingly recognized to play pivotal and intricate roles in promoting carcinoma invasion and metastasis in the past decade. However, there has been no systematic research on the effect and the specific mechanism of emotional disorder on the development and function of breast cancer thymus and TECs. Here, we used the chronic unpredictable mild stress to stimulate breast cancer mice and treated with RYF, and did a systematic study on the thymus morphology, pathological changes, functional changes and the expression levels of related factors in mice after administration. Then the potential molecular mechanisms were explored to explain RYF attenuates the thymus abnormal phenotypic changes and improved the thymus structure and output function on CUMS induced 4T1 breast cancer mice.

Table 1
Components of RYF.

Chinese name	Botanical name	Part used	Amounts (g)	Lot Number
Dang Shen	*Codonopsis pilosula* (Franch.) Nannf.	Root	15	200,101
Huang Qi	*Astragalus membranaceus* (Fisch.) *Bge.* Radix	Root	20	191,202
Dang Gui	*Angelica Sinensis* (Oliv.) Diels	Root	12	191,202
Chai Hu	*Bupleurum chinense* DC.	Root	12	191,201
Chuan Xiong	*Ligusticum chuanxiong* Hort.	Rhizome	6	191,001
Sheng Bai Shao	*Paeonia lactiflora* Pall.	Root	9	200,101
Lian Qiao	*Forsythia suspensa* (Thunb.) Vahl	Fruit	12	200,101
Gan Cao	*Glycyrrhiza uralensis* Fisch.	Rhizome	6	200,102
Gua Lou	*Trichosanthes kirilowii* Maxim.	Fruit	15	191,201
Qing Pi	*Citrus reticulata* Blanco	Fruit	6	190,701

2. Materials and methods

2.1. Chemicals and antibodies

Professor Tong-chuan He from the University of Chicago presented the mouse breast cancer cell line (4T1), Plasmid SSR#69 (designed by Professor Westerman), and PAMPHO plasmid. LipofectAMINE 2000 was purchased from Invitrogen (CA, USA). Calycosin-7-glucoside (111,920–201907), ferulic acid (110,773–201915), lobetyolin (111,732–201908), ligustilide (111,737–201910) were purchased from National Institutes for Food and Drug Control. Cyclophosphamide (CTX) was purchased from Shanghai Baxter Healthcare Co., Ltd. Hematoxylin and eosin (H&E), Serotonin/5-hydroxytryptamine (ST/5-HT) ELISA kit, DMSO were purchased from Shanghai Sangon Biotech Co., Ltd. Rat anti-Mouse CK5 antibody was purchased from Affinity Biosciences Pty Ltd. Rabbit anti-Mouse CK8 antibody, TSLP antibody, Goat Anti-Rabbit IgG were purchased from Abcam Shanghai Trading Co., Ltd. Rabbit anti-mouse CD3, Rabbit anti-mouse CD4, Rabbit anti-mouse CD8, FITC-rabbit anti-mouse E-cadherin were purchased from BD Pharmingen Co., Ltd. F (ab') 2-Goat Anti-Mouse IgG (H + L) Alexa Fluor 594, PE-Goat Anti-Mouse IgG were purchased from Thermo Fisher Scientific Co., Ltd. FITC-mouse anti-rabbit IgG, mouse anti-Rabbit IgG-FITC IgG, GAPDH antibody, p-STAT3 antibody were purchased from Santa Cruz Biotechnology (Shanghai) Co., Ltd. STAT3 antibody, p-JAK2 antibody, PI3 Kinase p110α antibody, p-PI3 Kinase p55/p85 antibody, rabbit anti-mouse Vimentin were purchased from CST Co. Ltd. DMEM, fetal bovine serum were purchased from Gibco Life Technologies. Hoechst 33,258 was purchased from Sigma-aldrich (Shanghai) Trading Co., Ltd. Rabbit anti-mouse enhanced polymer antibody was purchased from Zsbio Co., Ltd.

2.2. The preparation of RYF aqueous extract

The composition of RYF is showed in Table 1. All dried herbs were purchased from the Binjiang outpatient department of Zhejiang Chinese Medical University. The lot numbers were showed in Table 1. Prescription dosage of RYF was milled into powder and soaked in 8 times prescription dosage distilled water, and then extracted with boiling water under reflux for 2 h. The extract was filtered, and the extraction was repeated once. Subsequently, the filtrates were combined and evaporated under vacuum (RV8V, IKA, Werke GmbH & CO. KG, Staufen, Germany) and then lyophilized with a freeze dryer (VirTis, AD 2.0 EL, SP Scientific, USA) into powder. The yield of RYF aqueous extract was 9.61% (w/w) (He et al., 2021).

2.3. HPLC analysis

Chromatographic analysis was performed using a C_{18} column (250 mm × 4.6 μm, 5 μm; Waters) maintained 25 °C. A binary mobile phase consisting of acetonitrile (A) and water-acetic acid (B; 100:0.2, v/v) was used at a 1.0 mL/min flow rate. Gradient elution was performed according to the following elution program: 0–6 min, 10–20% A; 6–8 min, 20% A; 8–15 min, 20–23% A; 15–17 min, 23–25% A; 17–27 min, 25–50% A; 27–37 min, 50–80% A; 37–45 min, 85-10% A. The injection volume was 10 μL, and the detection wavelength was set at 284 nm. Each reference standard (calycosin-7-glucoside, ferulic acid, lobetyolin, ligustilide) was dissolved in methanol to prepare the stock solution. The lyophilized powder was accurately weighted (0.109 g), then dissolved in water (1.13 g dried herbs/mL), and the solution was centrifuged at 12,000 rpm for 10 min, and the 10 μL supernatant was injected into the HPLC system for analysis (He et al., 2021). The fingerprint similarity evaluation software is TCM chromatographic fingerprint Similarity Evaluation System 2012 Edition.

2.4. Cell culture and animals

Thymic epithelial cells (TECs) were obtained from BALB/c mice (Shen et al., 2020). All cell lines were cultured in DMEM containing 10% fetal bovine serum at 37 °C with 5% CO_2.

BALB/c mice (4–6 w, Female) were purchased from Shanghai Lab. Animal Research Center (license No. SCXK (Shanghai) 2017–0005) and maintained at the animal facility of Experimental Animal Research Center of Zhejiang Chinese Medical University (license No. SYXK (Zhejiang) 2021–0012), under standard conditions (room temperature, 24 ± 2 °C; humidity 50%–60%; 12 h light/dark cycle). This study was reviewed and approved by the Animal Ethics Committee of Zhejiang Chinese Medical University (IACUC-20210517-07). Fig. 1 shows the process of animal experiments.

2.5. Establishment of mice model

After two days of acclimatization, mice were lightly anesthetized and injected with 100 μL of 4T1 cell suspension subcutaneously into the 2nd pair mammary fat pad on the right at a cell density of 1.0×10^7 cells/mL (the normal group was injected with a vehicle of PBS). Two days after tumor inoculation, animals were randomly divided into five groups (n = 4) and give the mice a gavage: (i) cyclophosphamide group (30 mg/kg); (ii) model group (0.2 mL, normal saline); (iii) RYF-L (low concentration) group (1.45 g crude herbs/kg); (iv) RYF-M (medium concentration) group (2.90 g crude herbs/kg); (v) RYF-H (high concentration) group (5.80 g crude herbs/kg). Four health mice were prepared in a normal group (0.2 mL, normal saline). All treatments lasted for 20 days (He et al., 2021).

CUMS model mice were established by a CUMS method (Antoniuk et al., 2019; Dong et al., 2013) with some modifications. Thirty healthy BALB/c mice were selected, each with 6 mice, and they were divided into normal group, model group, CUMS group 1, CUMS group 2, and CUMS group 3. In addition to the normal group, the model group, the CUMS group were given 5 times unpredictable chronic stress stimuli per day (including: clip 3 min; 160 horizontal shaking per minute for 5 min; c for 3 h), 1 stimulus each time, randomly arranged so that the mice cannot predict the next stimulus to avoid adaptation, and co-stimulation for 35 days. Starting from 7 days after the mice received unpredictable chronic stimulation, except for the normal group, each mouse was inoculated with 100 μL 4T1 cell suspension (1×10^7/mL) under the second pair of breast pads on the right side to establish a CUMS-stimulated and 4T1 breast cancer mouse model. A significant decrease in brain 5-HT levels in mice indicates successful modeling. After the model is successfully established, give the mice a gavage with different concentrations of RYF (CUMS + L, CUMS + M, CUMS + H with 1.45, 2.90, 5.80 g/kg, respectively), CTX (30 mg/kg) or normal saline.

The diameter L (mm) and the short diameter W (mm) of the tumor were measured every 5 days after tumor implant. Tumor volumes (V, mm^3) were calculated with Equation (1). After the mice were sacrificed, thymus, spleen and tumor were dissected and weighed to calculate the organ index with Equation (2). The anti-tumor rate was evaluated by Equation (3). Observe the number of nodules on the lung surface after soaking the lungs with formalin for 48 h.

$$V = (L + W) \times L \times W \times 0.2618 \tag{1}$$

$$\text{Organ Index}(\%) = \frac{\text{visceral mass(g)}}{\text{body mass(g)}} \times 100\% \tag{2}$$

$$\text{Anti} - \text{tumor Rate}(\%) = \left(1 - \frac{\text{average tumor mass of experimental group(g)}}{\text{average tumor mass of control group(g)}}\right) \times 100\% \tag{3}$$

2.6. Open field test (OFT)

Thirty-five days after the model was established, the open-field test method was used for testing. Self-made square open box, with a bottom area of 50 cm × 50 cm, equally divided into 25 grids, and a box height of 50 cm. Record the time the mouse stays in the central area (9 grids in the middle) and the edge area (16 grids on the periphery of the central area are the edge areas). All 4 paws enter the square to start counting. The movement of the mice within 3 min was measured each time. Open field test video is analyzed with Smart 3.0 software.

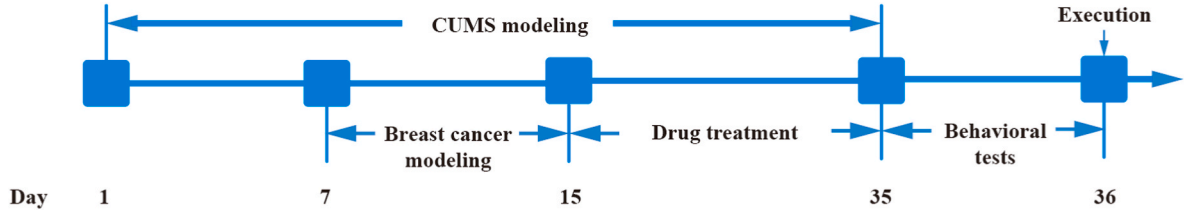

Fig. 1. Experimental design. Timeline of animal experiments, chronic unpredictablemild stress (CUMS) procedure, drugs administering, and behavioral tests.

2.7. Forced swim test (FST)

One day before the formal experiment, pre-experimental training for swimming. The mice are placed in a transparent glass drum with a height of about 30 cm and a diameter of 20 cm. The water depth is 150 cm and the water temperature is (25 ± 5) °C to ensure that the mice cannot jump out of the sink or Reach the bottom. In the formal forced swimming experiment, a video camera was used to record the 6-min swimming process, and the time of immobility (floating, upper body immobile, lower limbs treading water as immobility) in the last 4 min was counted. The video is analyzed with Smart 3.0 software.

2.8. ELISA

After 24 h of the experiment, the mice were sacrificed by neck removal, during which the mice were fasted. In the experiment, the eyeball was taken blood and then the head was decapitated, and 0.2 g of the mouse brain was homogenized in saline on an ice bath, and centrifuged to obtain the supernatant. The content of the neurotransmitter 5-HT in mouse brain was determined by ELISA according to the instructions of the enzyme-linked immunoassay kit.

2.9. H&E staining

Retrieved thymus tissues were fixed in 10% formalin and embedded in paraffin. Serial sections (about 4 μm thick) of the embedded specimens were stained with H&E for thymus tissue. The morphological changes of mouse thymus tissue were observed under light microscope (Motic, China) and the images were collected for analysis.

2.10. Immunofluorescence staining

Retrieved thymus tissues were fixed in 10% formalin and embedded in paraffin. Immunofluorescence staining was carried out for thymus tissue. Slides were deparaffinized and then rehydrated inagraduated fashion, the deparaffinized slides subjected to antigen retrieval. Then add Rat anti-Mouse CK5 (1:100) antibody and Rabbit anti-Mouse CK8 antibody (1:100), overnight at 4 °C in the refrigerator, secondary antibody FITC-Mouse anti-Rabbit IgG (1:100) antibody, PE-Goat Anti-Mouse IgG (1:100) antibody was incubated for 2 h at room temperature and protected from light, then the slides were mounted with anti-fluorescence quencher containing DAPI staining solution and observed with VS120-S6-W scanning analyzer (Olympus, Japan).

The cells were seeded on 24-well plates (3×10^4/well) for 24 h and were repeatedly washed with PBS. The sterile coverslips with cells were fixed in 4% paraformaldehyde (PFA) for 15 min. Then permeabilized with Triton-100, and blocked with 0.5% bovine serum albumin (BSA) for 40 min at room temperature. The cells were incubated with primary antibody, rabbit anti-mouse CK5 (1:100), rabbit anti-mouse CK8 (1:100), or FITC-rabbit anti-mouse E-cadherin (1:200), rabbit anti-mouse Vimentin (1:100) for overnight at 4 °C. The cells were followed by incubation with secondary antibodies, FITC-mouse anti-rabbit IgG (1:100) and PE-Goat Anti-Mouse IgG (1:100) at room temperature for 2 h. Cell nuclei were stained with Hoechst 33,258 (1 μg/mL) for 5 min. The labeled section was viewed with fluorescence confocal microscopy (Zeiss, Germany).

2.11. Flow cytometry analysis

After thymus was retrieved and thymocytes were isolated, all cells were resuspended in 200 μL PBS, washed with PBS, and blocked with 1% BSA at 4 °C for 20 min. Add antibodies CD3, CD4, CD8 and incubate on ice in the dark for 30 min. The data was collected on BD C6 and analyzed using FCS Express V3.

2.12. Cell proliferation analysis

The establishment and evaluation of iTECs were described in the literature (Shen et al., 2020). Logarithmically grown iTECs were seeded in 96-well plates (1×10^4/well). Cells were divided into different concentration treatment groups of RYF extraction (100 μl of 25, 50, 100, 200, and 400 μg/mL). There were no cells and only 100 μL cell cultural medium in the negative control group. The control group used 100 μL of cell cultural medium with 0.1% DMSO (Sangon Biotech) replaced RYF extraction. There were three wells of cells used as repeated in each group. The cells were incubated at 37 °C with 5% CO_2 for 48 h 20 μL of MTT solution (5 mg/mL) was added into each well. After 4 h incubation, the cell culture medium was discarded, and 150 μL of DMSO was added to each well. Plates were shaken at room temperature for 10 min. The absorbance value was measured at 570 nm using Synergy H1 Multi-Mode Microplate Reader (Bio-Tek, USA). And then calculated the inhibition rate of cell proliferation (%) with MTT assay.

Logarithmically grown iTECs cells were seeded in 24-well plates (3×10^4/well) for 24 h. There was 100 μL of cell culture medium with 0.1% DMSO added to the iTECs negative control group and different concentration treatment groups of RYF extraction (300 μL of 50, 100, and 200 μg/mL). The cells were incubated at 37 °C with 5% CO_2 for 48 h, and then the cell culture medium was discarded. 300 μL of crystal violet staining solution was added to each well and stained at room temperature for 30 min. Subsequently, repeated washed with water and dried naturally and then observed the proliferation. Results were expressed as a percentage of cell proliferation with respect to negative control group cells (as 100%) (He et al., 2021).

2.13. TGF-β1 induced EMT in iTECs

TGF-β1 was used to induce EMT of iTECs. Briefly, iTECs in the logarithmic growth phase were seeded in 24-well plates (3×10^4/well) for 24 h, and then starved with serum-free medium for 24 h. Cells were divided into five groups: (i) normal group (DMEM high sugar medium); (ii) TGF-β1 group (10 ng/mL TGF-β_1); (iii) RYF-L group (50 μg/mL RYF extraction and 10 ng/mL TGF-β_1); (iv) RYF-M group (100 μg/mL RYF extraction and 10 ng/mL TGF-β1); (v) RYF-H group (200 μg/mL RYF extraction and 10 ng/mL TGF-β1). There were three wells of cells used as repeated in each group. The TGF-β1 was administered first, then after 48 h, the RYF extraction was added and cultured for 24 h. The morphology of iTECs cells induced by TGF-β1 was observed with a microscope. The phenotype marker of E-cadherin and Vimentin was observed by immunofluorescence staining method described in 2.7. Quantitative real-time PCR analysis detected the expression level of Zeb-1 and Snail 1 and other mRNAs for phenotypic markers and phenotype-related transcription factors (He et al., 2021).

2.14. Immunohistochemical analysis

The paraffin sections were hydrated, dewaxed, and antigen retrieved, while then incubated with 3% hydrogen peroxide for 15 min to block endogenous peroxidase activity and washed with PBS three times. The sections were then incubated overnight with the primary antibody at 4 °C in a humid chamber with E-cadherin (Cell Signaling Technology) and Vimentin (Cell Signaling Technology). PBS was used as a negative control. The dilutions used for the primary antibodies were 1:200. The sections were subsequently incubated with rabbit anti-mouse enhanced polymer antibody at 37 °C for 2 h. Then the reaction products were developed with 3, 30-diaminobenzidine (DAB), counterstained with hematoxylin, differentiated with 1% hydrochloric acid ethanol, washed with distilled water, dehydrated with graded ethanol, vitrified by xylene and sealed with neutral gum. The stained sections were observed with a fluorescence microscope (Axio Scope. A1, Zeiss, Germany) after the sections dried.

2.15. Luciferase analysis

Logarithmically grown iTECs cells were seeded in 24-well plates (3×10^4/well) until the cell density reached 80%–90%. Then discarded the culture medium, washed with serum-free DMEM, added 1.2–2.0 mL serum-free DMEM, and put in the culture incubator for 20 min. The pBGLuc-Smad plasmid was infected and transfected by LipofectAMINE 2000. Subsequently, the successful infection and transfection iTECs were divided and treated by the method described in 2.12. The luciferase level of all groups of cell supernatant liquid (50 μL) was analyzed with a single-channel bioluminescent detector according to the Luciferase gene kit's instruction and calculated the relative activation degree of Smad pathway (%). The expression of Smad mRNA of each group was detected by PCR.

2.16. Realtime-PCR

After fresh EDTA anticoagulant blood was taken, total DNA of mouse peripheral blood mononuclear cell was extracted according to the instructions of the mammalian genomic DNA extraction kit. Total RNA of thymus was extracted by tissue RNA rapid extraction kit (Yishan Biology). The cells were seeded on 6-well plates (1×10^5/well) for 24 h, respectively. The steps of total RNA extraction, reverse transcription, and quantitative fluorescence detection of SV40 mRNA were described (Shen et al., 2020). And then reverse-transcribed using M-MuLV First Strand cDNA Synthesis Kit according to the manufacturer's instructions. An equal volume of DNA/cDNA was then used for Realtime-PCR using 2× SG Fast qPCR Master Mix and ABI7500 RT-PCR machine (ABI, USA). PCR amplification was performed with GAPDH as a reference to detect the expression of target mRNA by the $2^{-(\Delta\Delta Ct)}$ method in different group. PCR primers (Sangon Biotech, Shanghai, China) are showed in Table 2.

2.17. Western Blot

Total protein was extracted after the mouse thymus was completely removed, and the BCA protein assay kit was used to analyze the protein concentration. The total protein was separated by SDS-PAGE gel (P0012AC, Beyotime Biotechnology, China) was electrophoretically transferred to PVDF membranes and sealed for 1.5 h, Subsequently, the membranes were incubated overnight at 4 °C with the following primary antibodies: TSLP、JAK2、p-JAK2、STAT3、p-STAT3、PI3K、p-PI3K p55/p85. Goat anti-rabbit IgG (H + L) secondary antibody was incubated for 1 h at room temperature. ECL kit to makes colors appear, Bio-Rad's chemical imager to visualize the target protein band, Image J software was used to analyze the gray scale quantitation of Western blots, and GAPDH as the internal reference to calculate the protein change.

2.18. Statistical analysis

The statistical analysis was performed with SPSS 20.0 software, and the results were expressed as mean ± SD. One way ANOVA was used to compare the means of multiple groups, and the least significant difference test was used to compare the two groups. Differences were considered statistically significant when $P < 0.05$.

3. Results

3.1. HPLC analysis of RYF extract

Four components were analyzed and determined by HPLC by comparing them with the referenced solution. In Fig. 2A, No. 15 peak was calycosin-7-glucoside, No. 19 peak was ferulic acid, No. 20 peak was lobetyolin, and No. 29 peak was ligustilide. The concentrations were 1.2 ± 0.13 mg/g, 0.11 ± 0.03 mg/g, 0.11 ± 0.02 mg/g, and 0.018 ± 0.01 mg/g in dried herbs, respectively. In Fig. 2C, the similarity of fingerprints of sample 1, 2,3 was 1.000, 0.998, and 0.999, respectively.

3.2. Effects of RYF on 4T1 tumor-bearing mice and CUMS-stimulated tumor-bearing mice

3.2.1. Establishment of CUMS induced 4T1 breast cancer mice

3.2.1.1. Behavior of mice. Thirty five days after modeling, mice in the normal group and CTX group have bright coat color, strong body, agile movement, good autonomous mobility, and more autonomous activities; mice in model group, CUMS + L, CUMS + M and CUMS + H groups have rough fur, thin body shape, slow movement, and poor autonomy.

3.2.1.2. OFT and FST. In OFT, compared with the normal group, the central area stay time of the model group was longer; compared with the model group, the central area stay time of the CUMS + L group was slightly longer, while the stay time in CUMS + M and CUMS + H group was significantly shortened. In FST, compared with the normal group, the immobility time of the model group increased; compared with the model group, the immobility time of the mice in the CUMS + L and CUMS + M groups was slightly shortened, while the stay time of the CUMS + H group was prolonged. The results were showed in Fig. 3A.

Table 2
Primer sequences.

Gene name	Forward primers (5' - 3')	Reverse primers (5' - 3')
GAPDH (Mus)	GGCTGCCCAGAACATCAT	CGGACACATTGGGGGTAG
TSLP (Mus)	AGCCAGCTTGTCTCCTGAAA	GGCAAATGTTTTGTCGGGGA
STAT3 (Mus)	TAGTGTGCTCAGTTGTCCCC	GCCCTTCACGGTAACTCTCA
IL-5 (Mus)	AGGGACATCTCCTTGCAGTG	CACGGAGAAGTAAGGCCCAG
IL-6 (Mus)	GACAAAGCCAGAGTCCTTCAGA	TGACTCCAGCTTATCTCTTGGT
IL-7 (Mus)	TCTGCTGCCTGTCACATCATC	GGACATTGAATTCTTCACTGATATTCA
IL-10 (Mus)	TTGCTCCCATTCCTCGTCAC	GCAATGAATTCTAGGCTCAGGC
IL-12 (Mus)	AGACTCCCTGGACGTTTGTC	ATCGGCCTCTTCACACACAT
IL-1α(Mus)	AAGTCTCCAGGGCAGAGAGG	TTTCTTTGCCGACTCAAGCG
IL-17 (Mus)	CCTGGTGTTTAGCTGCTGGA	GGGTGCACTCGTGAAAACAC
TGF-β1 (Mus)	TCTCAGCGTGGTGAGGTATT	AGGCTTCATTTGTGGGAGCA
TNF-α(Mus)	TACAGCGACACTTGACACCC	TGCGGACCATAGAGAGTGGA
Foxp3 (Mus)	CCCATCCCCAGGAGTCTTGC	ACCATGACTAGGGGCACTGTA
TRECs(Mus)	CATTGCCTTTGAACCAAGCTG	TTATGCACAGGGTGCAGGTG
SV40	TCTTCGTCT CCG GCT CTG	CTGGCAACTTCATGCAAA
Snail 1	GTCCAGCTGTAACCATGCCT	TGTCACCAGGACAAATGGGG
E-cadherin	CAGCCGGTCTTTGAGGGATT	TGACGATGGTGTAGGCGATG
Vimentin	GGATCAGCTCACCAACGACA	AAGGTCAAGACGTGCCAGAG
Zeb 1	ACAAGCGAGAGGATCATGGC	CTGCTTTCTGCGCTTACACC
Smad 2	CCAGTTGTGAAGAGACTGCT	CGGAGGAGAGCAGAATGGGC

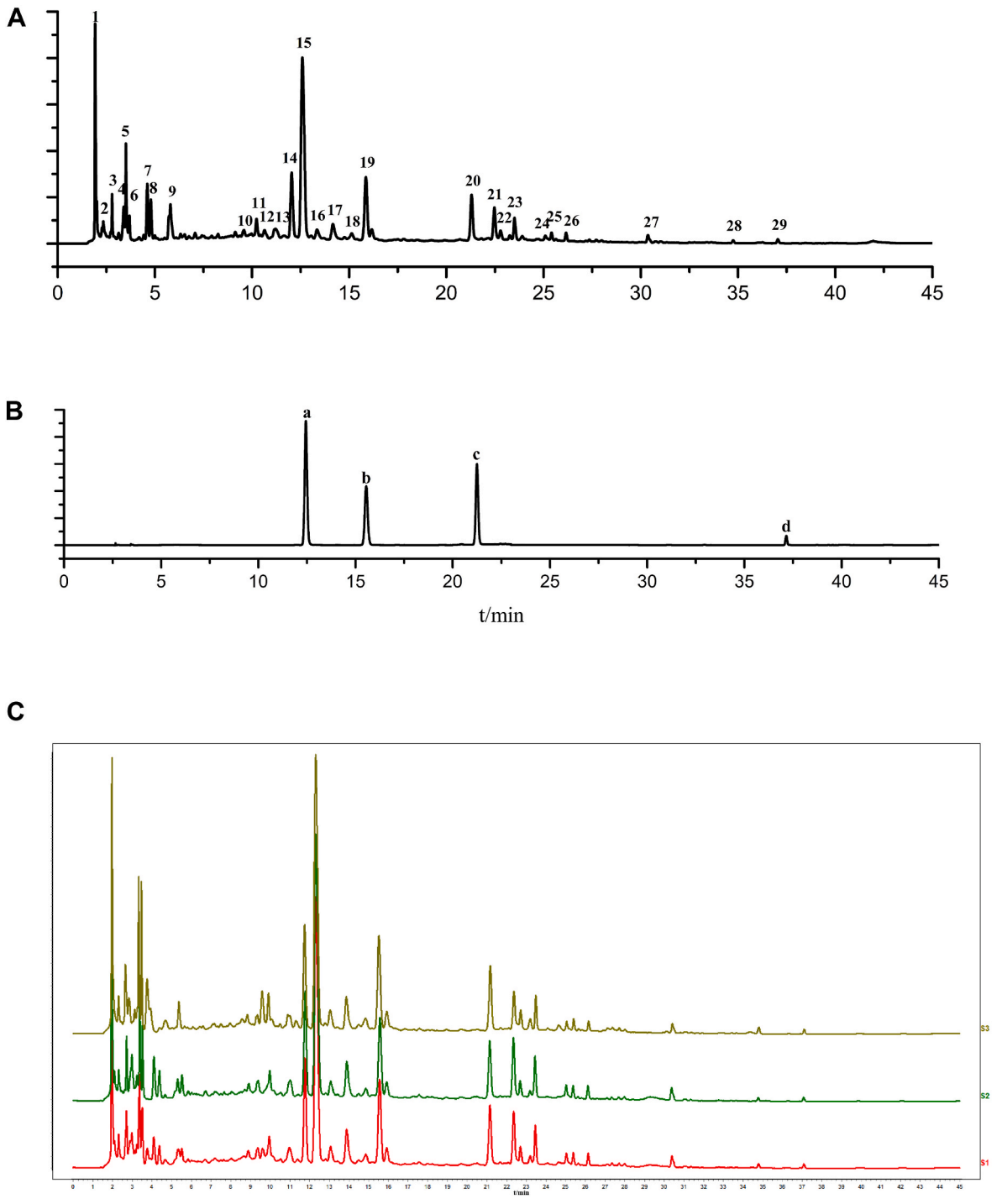

Fig. 2. (A) The HPLC fingerprint of RYF. (B) The HPLC chromatogram ofstandard reference solution. (References: a. calycosin-7-glucoside; b. ferulic acid; c. lobetyolin; d. ligustilide.) (C) The fingerprint profiles of three batches of the formula.

3.2.1.3. 5-HT in mice brain. Compared with the normal group, the content of 5-HT in the brain of the mice in the CUMS-stimulated tumor-bearing mice model group decreased, indicating that the level of 5-HT in the mice was disturbed after CUMS stimulation; compared with the model group, the 5-HT content of the mice in the administration group was significantly increased, indicating that RYF can increase the 5-HT content in the brain of mice that was reduced by CUMS stimulation (Fig. 3B).

3.3. RYF altered the index of lung, spleen, lymph node, thymus, and tumor

The lung, spleen, thymus, lymph node and tumor index in 4T1 tumor-bearing mice increased significantly compared with the normal group. Compared with the model group, the spleen, thymus, and tumor index in CTX group decreased significantly, and the antitumor rate was 51.33%. In addition, a significantly decrease appeared in spleen index of the RYF-L group and tumor index of RYF-M and RYF-H groups compared with the model group, and the antitumor rates in RYF-L, RYF-M, and RYF-H were 6.49%, 31.43%, and 33.45%, respectively. The results were

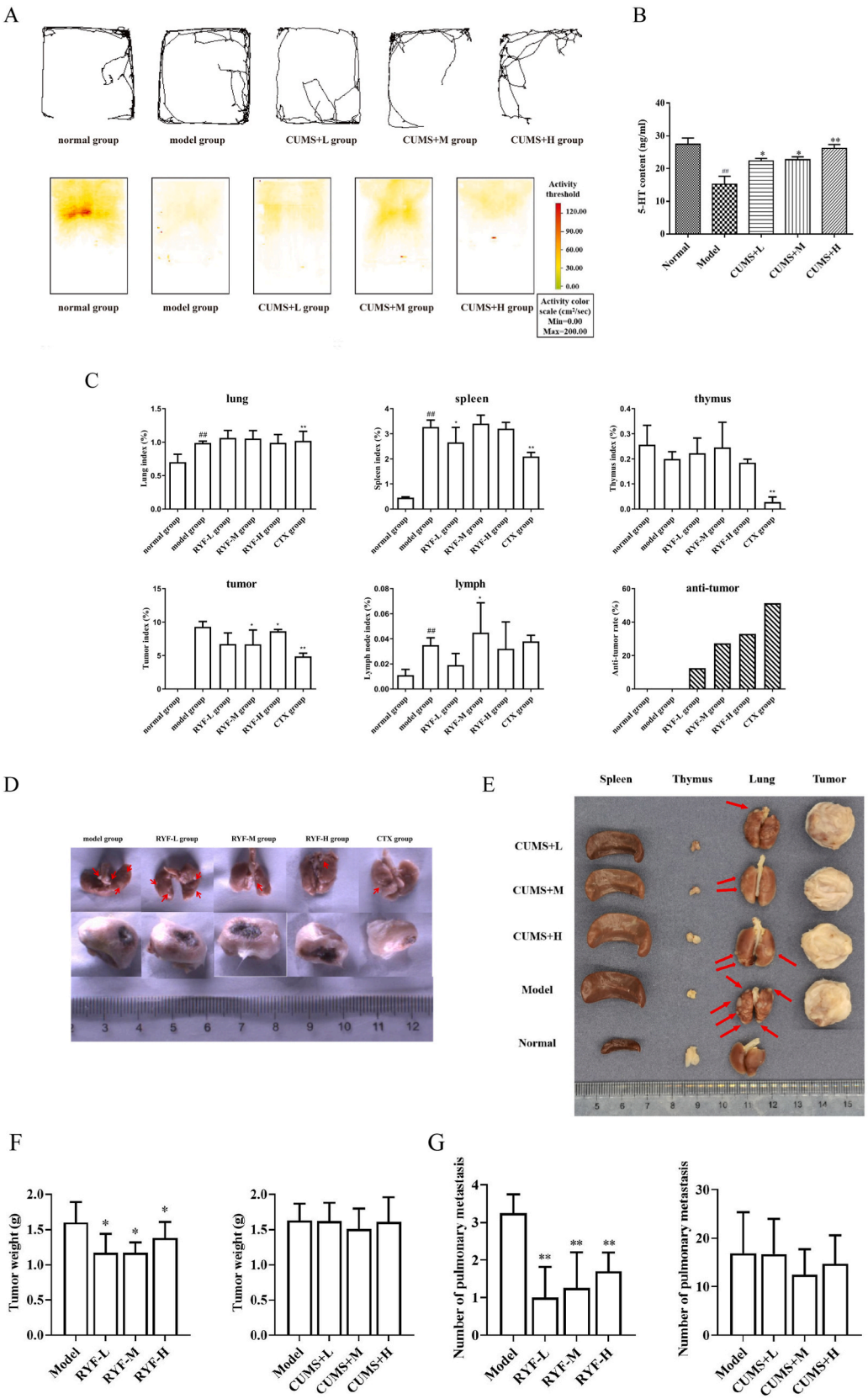

Fig. 3. (A) OFT and FST results of mice; (B) The content of 5-HT in the brain tissue of mice. (C)The organ index of lung, spleen, thymus, lymph node, and tumor index of different group changes on organs of 4T1 tumor-bearing mice. (D) The lung and tumor tissue in each group of 4T1 tumor-bearing mice; (E)The lung, spleen,thymus and tumor tissue in each group of CUMS-stimulated tumor-bearing mice. (F) The tumor weight in each group of 4T1 tumor-bearing mice and CUMS-stimulated tumor-bearing mice. (G) The number of pulmonary metastasis nodules in each group of 4T1 tumor-bearing mice and CUMS-stimulated tumor-bearing mice. Compared with normal group, $^{\#}P < 0.05$, $^{\#\#}P < 0.01$, compared with model group, $^{*}P < 0.05$, $^{**}P < 0.01$. Note: The red arrows indicate the tumor metastasis sites.

showed in Fig. 3CD.

As showed Fig. 3DEFG, compared with the normal group, the spleen size of the mice in the model group was increased obviously and the thymus size was decreased after CUMS stimulated. Compare with the 4T1 tumor-bearing mice model group, the tumor weights significant reducing after RYF treating. In CUMS-stimulated tumor-bearing mice group, the tumor weights reduced, but there were no significant difference. The pulmonary metastasis rates in the 4T1 tumor-bearing mice group were 100%, and after RYF treating, the number of pulmonary metastasis nodules significant reduced in all groups. In CUMS-stimulated tumor-bearing mice groups, the number of pulmonary metastasis nodules decreased, but there were no significant difference. In Table 3 and Table 4, the tumor volume reduced after day 14 in each group compared with corresponding model group. Moreover, there were significant reduction in 4T1 tumor-bearing mice groups after RYF treating.

3.4. RYF improved the thymus structure and output function of CUMS induced 4T1 breast cancer mice

3.4.1. RYF improved the thymus structure

The results of HE staining showed that in the thymus tissue of the normal group mice, the cortex and medulla were clearly demarcated, the cells were arranged in an orderly manner, and more thymocytes could be observed; The thymic lymphocytes of the mice in the model group were lost, the number of lymphocytes was reduced, the junction between the cortex and the thymus was blurred, and the structure of the thymus was disordered, which showed that the thymic cortex appeared atrophy. Compared with the model group, the number of lymphocytes in the CUMS + L group was further reduced, and there was no obvious cortical-medullary boundary. The thymus in the CTX group and the CUMS + H group were atrophied and degenerated, the density of lymphocytes decreased, and some areas were encapsulated by fat, and fat vacuoles appeared, showing obvious cortical-medulla demarcation. There was no lipid deposition area in the CUMS + M group, the morphology was relatively intact, the number of lymphocytes was large, and the boundary between the cortex and the medulla was obvious (Fig. 4A and B).

The results of immunofluorescence showed that compared with the normal group, the number of TECs in the medulla (mTECs, $CK5^+$) of the mice thymus in the model group decreased and in the cortex (cTECs, $CK8^+$) was increased; compared with the model group, the number of mTECs in each RYF group was increased, the TECs were evenly distributed. It is suggested that RYF can improve the atrophy of TECs in the medulla and maintain the activity of TECs (Fig. 4C).

In addition, the results of flow cytometry showed that compared with the normal group, the percentages of $CD3^+CD4^+CD8^-$ and $CD3^+CD4^-CD8^+$ T cells in the thymus of the mice in the model group were significantly increased, and the percentages of $CD3^+CD4^-CD8^-$ and $CD3^+CD4^+CD8^+$ T cells was significantly decreased; compared with the model group, the percentages of $CD3^+CD4^+CD8^-$ and $CD3^+CD4^-CD8^+$ T cells in each group treated with RYF were decreased,

Table 3
The tumor volume in each group of 4T1 tumor-bearing mice ($\bar{x}$ ±s, n = 4).

Tomor volume (mm^3)	Day 7	Day 14	Day 21	Day 28
Model	183.91 ± 41.2	365.88 ± 68.69	571.29 ± 209.53	963.2 ± 255.19
RYF-L	206.62 ± 45.8	468.55 ± 151.64	533.83 ± 119.59	907.72 ± 286.41
RYF-M	111.95 ± 71.29	253.3 ± 83.88*	376.1 ± 65.48**	897.93 ± 276.91*
RYF-H	117.87 ± 28.47	228.09 ± 64**	406.69 ± 151.96*	591.54 ± 157.67**

Note: *$P < 0.05$, **$P < 0.01$ compared with the model group.

Table 4
The tumor volume in each group of CUMS-stimulated tumor-bearing mice ($\bar{x}$ ±s, n = 8).

Tomor volume (mm^3)	Day 7	Day 14	Day 21	Day 28
Model	299.31 ± 33.17	697.33 ± 53.17	1053.56 ± 114.98	1974.79 ± 332.38
CUMS + L	272.59 ± 55.57	598.47 ± 108.95	936.17 ± 149.25	1677.63 ± 251.42
CUMS + M	303.22 ± 58.43	602.72 ± 87.76	942.39 ± 161.12	1813.32 ± 271.36
CUMS + H	304.07 ± 101.61	645.87 ± 199.65	1020.72 ± 328.14	1688.52 ± 451.11

and the percentages of $CD3^+CD4^-CD8^-$ T cells were increased, while the proportion of $CD3^+CD4^+CD8^+$ T cells in the CUMS+L and CUMS + H groups was further reduced on the basis of the model group (Fig. 4D). It suggests that the structure of the thymus is disturbed by tumors and chronic stress, and the positive selection function of the thymus and the export of mature T cells to the peripheral blood are inhibited, while RYF can, to a certain extent, promote the positive selection of the thymus with inhibited function and the output of mature T cells to the peripheral blood, thereby restoring the thymus structure to a certain extent.

3.4.2. RYF enhanced the thymic output function

Compared with the normal group, the expression of TRECs in the peripheral blood of the model group was significantly decreased; compared with the model group, the expression of TRECs in the peripheral blood of the mice in the CUMS + M group was significantly increased, suggesting that RYF could improve the short-term thymic output function of the CUMS-stimulated tumor-bearing mice (Fig. 4E).

3.5. RYF attenuates the thymus abnormal phenotypic changes of breast cancer mice by inhibiting the TGF-β1/smad pathway

3.5.1. RYF promoted the proliferation of iTECs and altered the morphology of iTECs after TGF-β1 treatment

MTT assay results showed that RYF treatment promoted the proliferation of iTECs (Fig. 5A). The cell proliferation rate of RYF-treated groups increased significantly compared with the control group in a dose-dependent manner.

The morphology observation (Fig. 5B) results showed that iTECs were short fusiform and lined up tightly in the normal group. Besides, the number of iTECs induced by TGF-β1 reduced, and intercellular spaces got less with the morphology changed to longer fusiform. Simultaneously, RYF treated could reverse the change of intercellular space and morphology.

3.5.2. RYF influenced the expression of E-cadherin and Vimentin in thymus tissue

The E-cadherin positive cells in the model group reduced significantly, and Vimentin positive cells increased notably compared with the normal group. Conversely, compared with the model group, the cells with E-cadherin positive expression increased, and with Vimentin positive expression reduced in RYF-treated group and CTX group (Fig. 5C and D).

3.5.3. RYF influenced the mRNA levels and protein expressions of E-cadherin, Vimentin, snail 1, and Zeb1 in TGF-β1 induced iTECs

E-cadherin is the characteristic marker of epithelial cells, and vimentin is the mark of interstitial cells. As seen in Fig. 5E and F, immunofluorescence staining results showed the target proteins presented in green fluorescence and the cell nucleus presented in blue.

Compared with the normal group, the E-cadherin's expression and mRNA level decreased, and Vimentin's expression and mRNA level were upregulation in TGF-β1 group. Moreover, the mRNA level of Snail 1 and

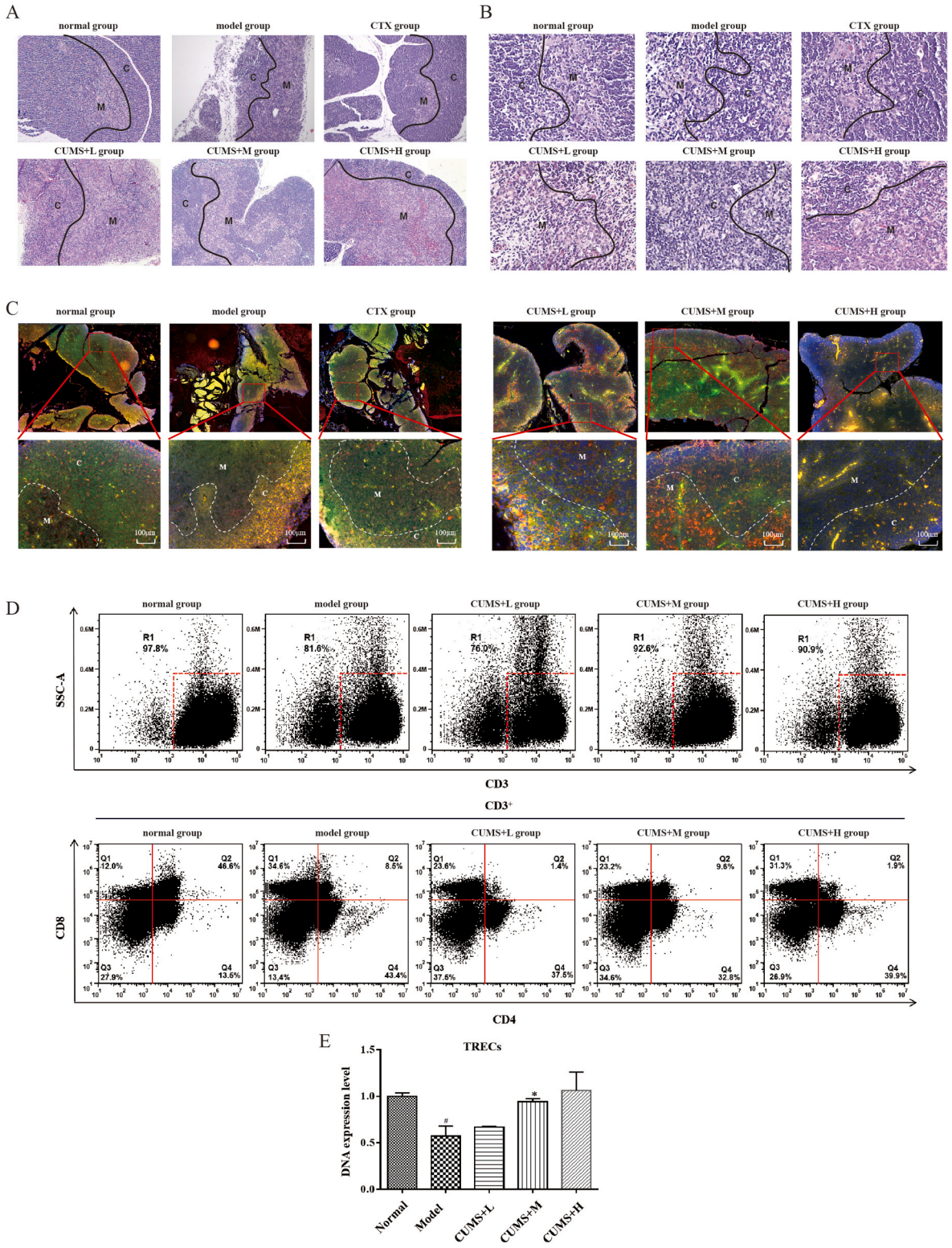

Fig. 4. (A) HE staining of thymus sections 100 × and (B) 400 × . (C) Immunofluorescence staining of thymus sections. Colocalization of TEC cells using CK5 (red fluorescence) and CK8 (green fluorescence) and zoom in on the area inside the red box. (D) T cell subset ratio in mice thymus. (E) Expression levels of TRECs DNA in peripheral blood of mice. Compared with normal group, $^{\#}P < 0.05$, $^{\#\#}P < 0.01$, compared with model group, $^{*}P < 0.05$, $^{**}P < 0.01$. Note: C: cortex, M: medulla.

Zeb 1 increased significantly. Furthermore, compared with the TGF-β1 group, RYF-treated group reversed the change in relative protein expression and mRNA levels. The results shown in Fig. 5G.

3.5.4. *RYF affected the smad pathway*

As showed in Fig. 5G, PCR results suggested that the level of Smad mRNA was upregulated significantly compared with the normal group in iTECs after TGF-β1 induced. Interestingly, the level of Smad2 mRNA was downregulated after RYF treating compared to the TGF-β1 group

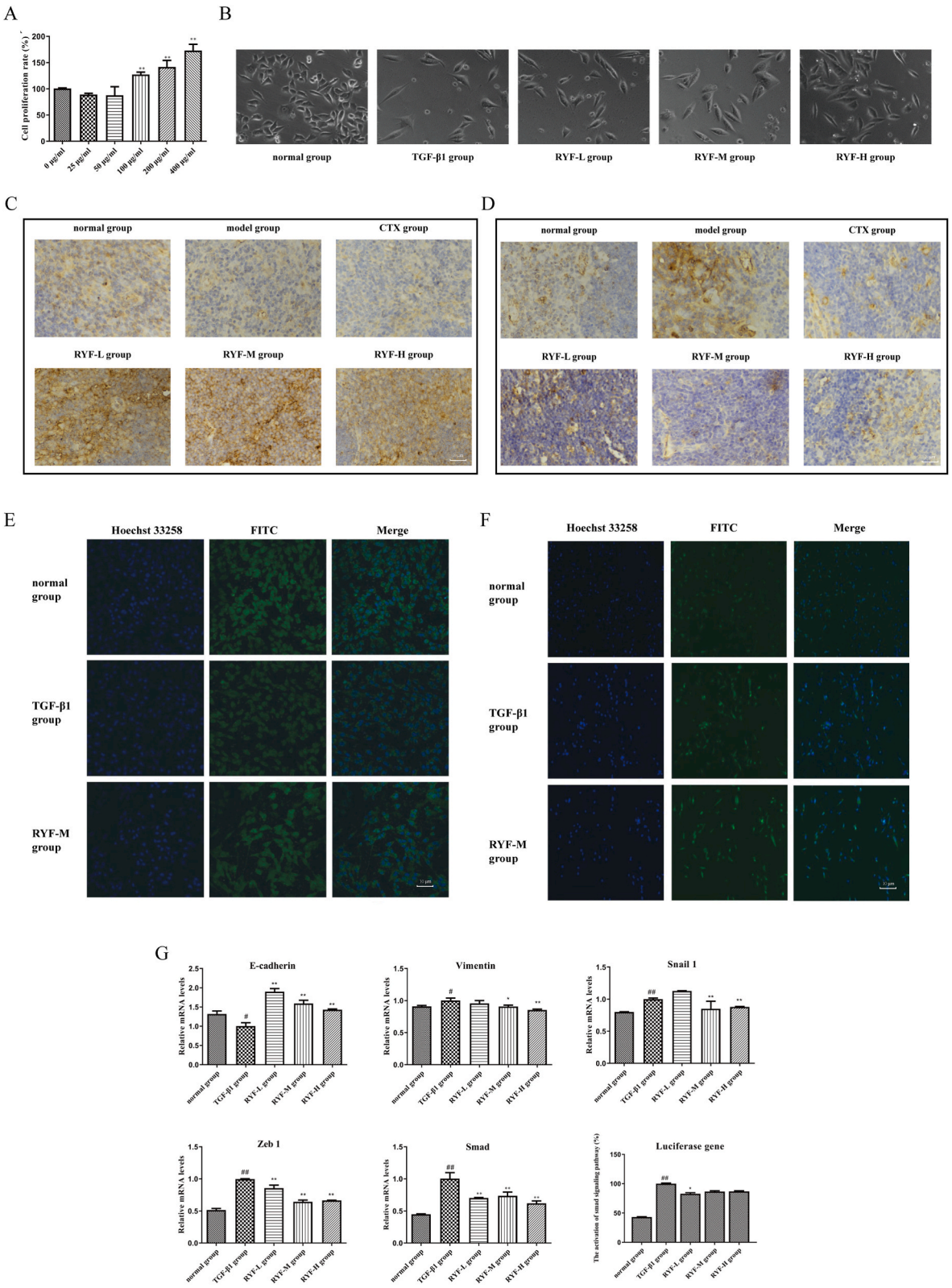

Fig. 5. (A) iTECs proliferation rate after treated by different concentrations of RYF. The data are presented as the mean ± SD ($n = 3$). $^{*}P < 0.05$, $^{**}P < 0.01$ compared to the 0 μg/mL group. (B) Cell morphology images of iTECs in different groups for 48 h (Magnification: 200×). The expression of E-cadherin (C) and Vimentin (D) in thymus tissue (Magnification: 100×). Immunofluorescence staining section of E-Cadherin (E), Vimentin (F) protein mRNA expression of iTECs in different groups (Magnification: 200×). (G) The mRNA levels of E-cadherin, Vimentin, Snail 1, Zeb 1, Smad 2 and luciferase gene detection results in iTECs of different groups. The data are presented as the mean ± SD ($n = 3$). $^{\#}P < 0.05$, $^{\#\#}P < 0.01$ compared to the normal group. $^{*}P < 0.05$, $^{**}P < 0.01$ compared to the TGF-β1 group.

and the differences were considered statistically significant ($P < 0.01$).

Luciferase assay results showed luciferase expression increased significantly in TGF-β1 group than in the normal group, indicating that the Smad pathway got activated. Furthermore, the luciferase expression in RYF-treated groups was downregulated. The differences between RYF-L and TGF-β1 groups were considered statistically significant ($P < 0.05$).

3.6. RYF restored the structure and function of the thymus by activating the JAK2/STAT3/PI3K pathway

3.6.1. The expression of TSLP, Foxp3, IL-1α, IL-5, IL-6, IL-7, IL-10, IL-12, IL-17, STAT3, TGFβ1 and TNFα mRNA in thymus

Compared with the normal group, Foxp3, IL-1α, IL-5, IL-6, IL-7, IL-10, IL-12, IL-17, STAT3, TGFβ1 and TNFα in the thymus of mice in the model group mRNA levels were significantly decreased, while TSLP was significantly increased. Compared with the model group, the mRNA levels of all factors in the thymus of mice in the CUMS + L group were increased to varying degrees. Except for TSLP, the mRNA levels of the other factors in the CUMS + M group were significantly increased, while the CUMS + H group except Foxp3. The levels of IL-7 and TSLP were significantly decreased, and the levels of other factors were further increased (Fig. 6A).

3.6.2. The level of TSLP、JAK2、p-JAK2、STAT3、p-STAT3、PI3K、p-PI3K protein in thymus

Compared with the normal group, the expressions of p-JAK2, PI3K, p-PI3K p85 in the thymus of the model group were increased, while the expressions of p-PI3K p55 and p-STAT3 were decreased; The expressions of p-STAT3, p-PI3K p85 and p-JAK2 were increased, and the expression of TSLP was decreased in the CUMS + L and CUMS + H groups, suggesting that RYF could alleviate the inhibitory effect of CUMS stimulation on the JAK2/STAT3/PI3K pathway in the thymus of tumor-bearing mice (Fig. 6B).

4. Discussion

Breast cancer is often accompanied by anxiety and depression symptoms (Greenlee et al., 2017). At the same time, depression will further promote the deterioration of the tumor, greatly reduce the patient's compliance with treatment and affect the treatment effect (Chirico et al., 2020). The evidence is strong for the association of depression with changes in Th17 cells (Beurel et al., 2022). Our experimental results showed that CUMS-stimulated could further promote the pulmonary metastasis of the cancer and the tumor volumes. However, how emotional disorders promote the occurrence and development of breast cancer is still lack of reliable scientific basis.

TGF-β has been widely used to induce phenotypic changes of epithelial cells and mediates the transformation of epithelial cells into mesenchymal cells, thus inhibiting the migration of tumor cells. As an important development process of cell adhesion and migration during tumor invasion, the hallmark of EMT is the functional loss of E-cadherin (Gloushankova et al., 2018; Peinado et al., 2007). Vimentin is an intermediate filament characteristically present only in certain epithelial of mesenchymal cells (Fraga et al., 1998). In general, E-cadherin is an epithelial marker and Vimentin is regarded as the mesenchymal marker (Akhtar et al., 2016). Afterwards, this study brings out the decrease of E-cadherin's expression and up-regulation of Vimentin in 4T1 tumor-bearing mice, which meant the TECs atrophy in thymus. Moreover, as two key transcription factors for cell motility, Snail and Zeb trigger EMT by repression epithelial markers and activation mesenchymal properties, and Smad signaling pathways are necessary for EMT (Medici et al., 2006). Therefore, we obtained the level of Snail 1, Zeb 1and Smad increased significantly in TGF-β1 group, and in RYF-treated groups, the expressions were reversed. It is suggested that RYF could confront the phenotypic transition of iTECs induced by TGF-β1, and its mechanism is related to the inhibition of the Smad pathway.

The disordered mood was evaluated with increasing 5-HT levels in the brains of the mice. 5-HT is an important neurotransmitter in the central system and participates in physiological responses such as sleep, mental activity, and emotional changes. Disrupting the release and re-absorption of 5-HT will lead to depressive disorders (Dell'Osso et al., 2016). The open field test and forced swimming test can reflect the spontaneous behavior, exploration activities and emotional reactions of mice, and are ideal evaluation criteria for depression. Therefore, we employed these methods to detect emotional changes in mice after stress. Our experimental results showed that the level of 5-HT in the brains of tumor-bearing mice stimulated by CUMS was significantly decreased, and the immobility time of forced swimming was prolonged, indicating that the mice developed disorders such as depression. The 5-HT levels in the brains of the mice were significantly increased after administration of RYF, and the immobility time in forced swimming was shortened, and the stay time in the central area of the open field experiment was shortened, indicating that the disordered mood of the mice was improved.

By observing the distribution of CK5 and CK8 in the mice thymus, detecting the level of TRECs in the peripheral blood of the mouse and the proportion of T cell subsets in the thymus, the changes in the structure and output function of the mouse thymus can be comprehensively evaluated. TECs are the most important thymic stromal cells in the thymus, which provide the most suitable survival for the development of thymocytes and are the basis for the functioning of the thymus (Nitta and Suzuki, 2016). CK5 and CK8 in TECs are specific markers of TECs and can be used to localize the distribution of TECs in the thymus (Bertho et al., 1997; Calderón and Boehm, 2012; Mohammad et al., 2009; O'Rourke et al., 2016). TRECs are by-products of T cell receptor (TCR) gene rearrangement and are closely related to the output function of the thymus. By quantitatively analyzing the level of TRECs in a unit number of T cells in a sample, it is possible to detect the number of T cells that have recently been exported by the thymus, thereby reflecting the export function of the thymus (Gennery, 2018; Ravkov et al., 2017). At the same time, the normal state of the body's immune function depends on the balance of the number and proportion of T cell subsets. CD3 is a marker on the surface of all T cells, while $CD4^+$ T cells with helper function and $CD8^+$ T cells with killing function are the two most important subgroups of T cells, which play an important role in thymocyte immune regulation (Lim et al., 2018; Nobrega et al., 2013). After CUMS stimulation, the spleen index was increased, and the thymus weight decreased. In our study, the percentages of $CD3^+CD4^+CD8^-$ and $CD3^+CD4^-CD8^+$ (Single positive, SP) T cells in the thymus of tumor-bearing mice under CUMS stimulation were increased, and the proportion of $CD3^+CD4^-CD8^-$ (Double negative, DN) and $CD3^+CD4^+CD8^+$ (Double positive, DP) T cells were decreased, in addition, the level of TRECs decreased, indicating that the positive selection function of the thymus and the export of mature T cells to peripheral blood were inhibited.

IL-7 can promote the differentiation of T cells, maintain the differentiation of naive T cells in the thymus, and participate in maintaining the homeostasis of peripheral $CD4^+$, $CD8^+$ T cells, helper cells and other immune cells (Marković and Savvides, 2020). As an IL-7-like cytokine, TSLP can regulate immature dendritic cell (DC) activation, $CD4^+$ T cell homeostasis and regulatory T cell development (Corren et al., 2019; Pattarini et al., 2017). Foxp3, IL-1α, IL-12, IL-6, IL-5, IL-10, IL-17, STAT3, TGF-β1 and TNF-α also participate in the immune regulation of the body. Studies have shown that the expression of Foxp3, IL-1α, IL-6, IL-12, IL-17, STAT3, IL-10, TNF-α, TGF-β1 and other factors will be significantly up-regulated in breast cancer (Ahmad et al., 2018; Cruceriu et al., 2020; Douglass et al., 2012; Jo et al., 2020; Kaplanov et al., 2019; Y. Ma et al., 2017; Siersbæk et al., 2020), while our study found that the changes of these factors were consistent, and no specific changes were found, so further study was not carried out. TSLP can in turn phosphorylate each other and intracellular receptors by activating Janus

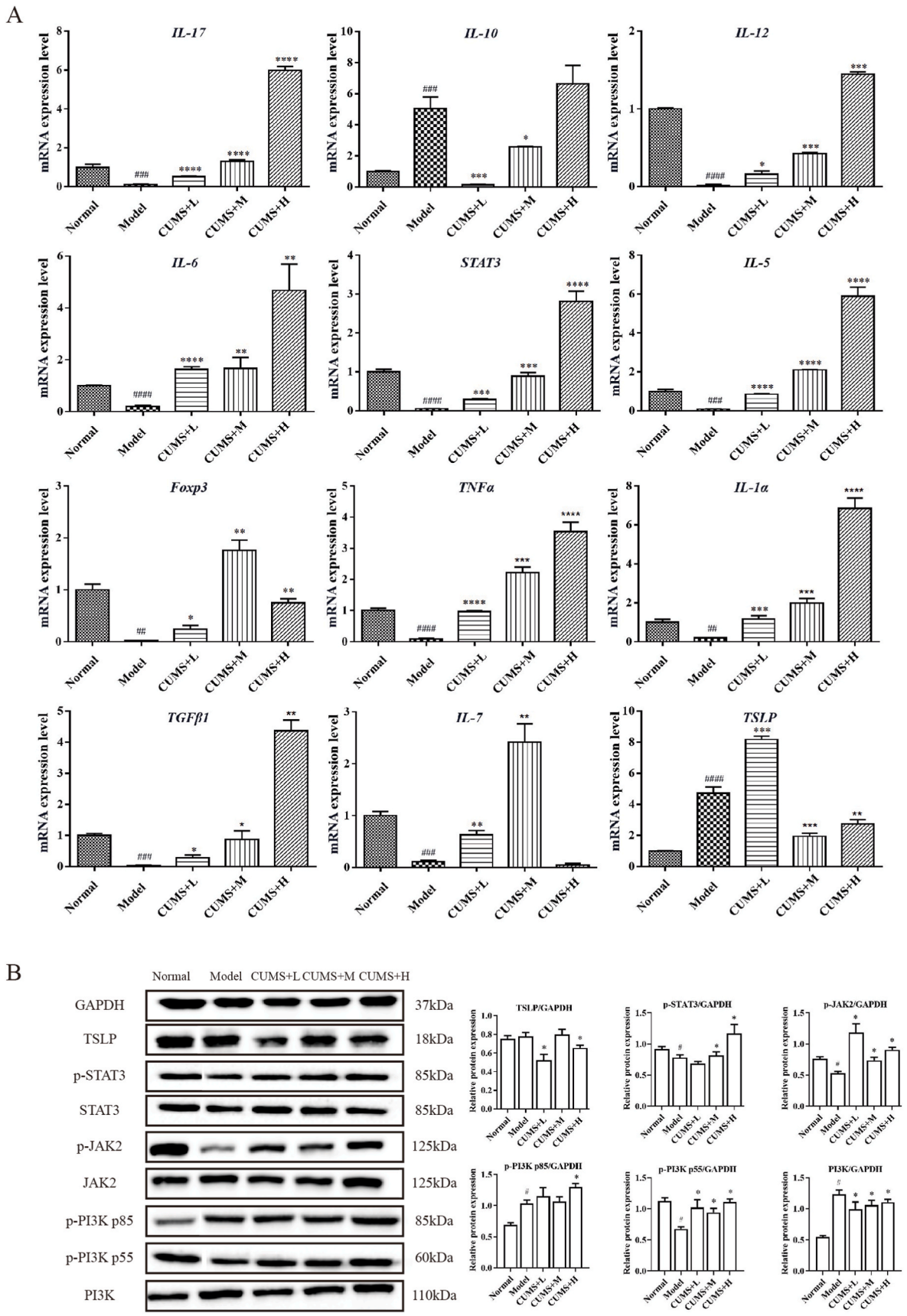

Fig. 6. (A) TSLP, Foxp3, IL-1α, IL-5, IL-6, IL-7, IL-10, IL-12, IL-17, STAT3, TGFβ1 and TNFα mRNA expression in thymus. (B) Expressions of TSLP and IL-7 downstream protein in thymus. Compared with normal group, $^{\#}P < 0.05$, $^{\#\#}P < 0.01$, $^{\#\#\#}P < 0.001$, $^{\#\#\#\#}P < 0.0001$; compared with model group, $^{**}P < 0.01$, $^{***}P < 0.001$, $^{****}P < 0.0001$.

kinase (JAK), which creates a docking site for Signal transducer and activator of transcription (STAT), these sites are recruited to receptors and phosphorylated by JAK on their tyrosine residues (Roan et al., 2012; Wohlmann et al., 2010). Phosphorylation of STAT results in dissociation from receptors, formation of homodimers or heterodimers with other STAT proteins, and nuclear translocation. In the nucleus, STATs regulate target gene transcription by binding to promoter or enhancer motifs or other noncoding intragenic and intergenic regions (Quentmeier et al., 2001). Among them, STAT3 is involved in cell proliferation and differentiation, plays a role in allergic inflammation, and also plays an important role in the differentiation of Th17 cells to produce IL-17 (Schindler et al., 2007; Yamanaka et al., 1996; M. Zhang et al., 2020). JAK2 is a member of the c-Jun N-terminal kinase (JNK) family and is involved in the signal transduction of many cytokines and growth factors. The JAK2/STAT3 signaling pathway is involved in the regulation of breast cancer cell proliferation (Yang et al., 2007). Meanwhile, the PI3K/AKT signaling pathway is closely related to cell survival and proliferation, differentiation and apoptosis (Y. J. Wu et al., 2016; Zhou et al., 2017). Studies have shown that activation of both STAT and PI3K/AKT signaling can be mediated through JAK (Gao et al., 2017; Ke et al., 2017; Lu et al., 2008). To this end, we selected JAK2/STAT3/PI3K pathway for further research and validation.

From the results of qPCR, CUMS stimulation inhibited the JAK2/PI3K pathway activated by breast cancer. After administration of RYF, although there was no significant change in the quality of the thymus, the number of lymphocytes in the thymus increased, the boundary between the cortex and the medulla was obvious, the structure of the thymus was restored to a certain extent. The percentages of SP cells in mouse thymus were decreased, and the percentage of DP cells was increased, and the output function of the thymus was enhanced. The number of TECs in the medulla of the mouse thymus was increased and evenly distributed, while the expression levels of markers CK5 and CK8 were both increased, indicating that the atrophy of epithelial tissue was significantly improved. In addition, in the results of qPCR and Western Blot, the expression level of IL-7 mRNA was significantly increased, the level of *TSLP* was significantly decreased, the protein expression of p-STAT3, p-PI3K p55 and p-JAK2 was increased, and the protein expression of TSLP was decreased after treated with RYF. It is shown that RYF can reduce the expression of TSLP and increase IL-7 in the thymus of CUMS-stimulated breast cancer mice, and promote the activation of the JAK2/STAT3/PI3K pathway, thereby inhibiting the pulmonary metastasis and development process of breast cancer.

5. Conclusion

Depression further promotes the pulmonary metastasis of the cancer nodules of the cancer and the tumor volumes, greatly increasing the risk of tumor progression. The thymic function of the tumor-bearing body was markedly abnormal, which was mainly due to the disorder of cortex and medulla region cells and atrophy of the medulla. Interestingly, RYF could reverse the phenotypic changes of TECs by down-regulating the expression of Snail 1 and Zeb 1 and inhibiting TGF-β1-induced Smad pathway. Furthermore, RYF can maintain the structure and output function of the mouse thymus to a certain extent by reducing the expression of TSLP in the thymus of CUMS-stimulated breast cancer mice, and at the same time promoting the activation of the JAK2/STAT3/PI3K pathway, thereby inhibiting the pulmonary metastasis and development process of breast cancer.

Funding

This work was supported by the Zhejiang Provincial Natural Science Foundation of China (grant numbers LGC20B050010, LY22H160007), opening fund of the State Key Laboratory of Quality Research in Chinese Medicine, University of Macau, Macau (grant number QRCM-OP21002), Zhejiang Provincial Key Laboratory Project of China (grant number 2012E10002), and National Natural Science Foundation of China (grant number 82274621).

CRediT authorship contribution statement

Bingqian He: Formal analysis, Writing – original draft, Writing – review & editing, Funding acquisition. **Wenqin Guo:** Methodology, Validation, Formal analysis. **Rongzhen Shi:** Methodology, Validation, Formal analysis. **Robert D. Hoffman:** Writing – review & editing. **Qihan Luo:** Investigation, Formal analysis. **Yuan-Jia Hu:** Conceptualization, Funding acquisition. **Jianli Gao:** Conceptualization, Writing – review & editing, Supervision, Funding acquisition, All authors read and approved the final manuscript.

Declaration of competing interest

The authors declare that they have no known competing financial interests or personal relationships that could have appeared to influence the work reported in this paper.

Data availability

Data will be made available on request.

Acknowledgements

We appreciate the great technical support from the Public Platform of Pharmaceutical Research Center, Academy of Chinese Medical Science, Zhejiang Chinese Medical University.

References

Ahmad, N., Ammar, A., Storr, S.J., et al., 2018. IL-6 and IL-10 are associated with good prognosis in early stage invasive breast cancer patients. Cancer Immunol. Immunother. 67, 537–549. https://doi.org/10.1007/s00262-017-2106-8.

Akhtar, K., Ara, A., Siddiqui, S.A., et al., 2016. Transition of immunohistochemical expression of E-cadherin and vimentin from premalignant to malignant lesions of oral cavity and oropharynx. Oman Med. J. 31, 165–169. https://doi.org/10.5001/omj.2016.33.

Alvarez-Mon, M.A., Gomez-Lahoz, A.M., Orozco, A., et al., 2021. Expansion of CD4 T lymphocytes expressing interleukin 17 and tumor necrosis factor in patients with major depressive disorder. J. Personalized Med. 11 https://doi.org/10.3390/jpm11030220.

Alvarez-Mon, M.A., Gómez-Lahoz, A.M., Orozco, A., et al., 2020. Blunted expansion of regulatory T lymphocytes is associated with increased bacterial translocation in patients with major depressive disorder. Front. Psychiatr. 11, 591962 https://doi.org/10.3389/fpsyt.2020.591962.

Antoniuk, S., Bijata, M., Ponimaskin, E., et al., 2019. Chronic unpredictable mild stress for modeling depression in rodents: meta-analysis of model reliability. Neurosci. Biobehav. Rev. 99, 101–116. https://doi.org/10.1016/j.neubiorev.2018.12.002.

Bao, Y.J., Tian, C.Y., Zheng, W., 2014. Combination of formula and massage treatment for the treatment of 76 cases of acute mastitis. Shanghai J. Tradit. Chin. Med. 48, 65–66. https://doi.org/10.16305/j.1007-1334.2014.08.022.

Bertho, J.M., Demarquay, C., Moulian, N., et al., 1997. Phenotypic and immunohistological analyses of the human adult thymus: evidence for an active thymus during adult life. Cell. Immunol. 179, 30–40. https://doi.org/10.1006/cimm.1997.1148.

Beurel, E., Medina-Rodriguez, E.M., Jope, R.S., 2022. Targeting the adaptive immune system in depression: focus on T helper 17 cells. Pharmacol. Rev. 74, 373–386. https://doi.org/10.1124/pharmrev.120.000256.

Boorman, E., Zajkowska, Z., Ahmed, R., et al., 2016. Crosstalk between endocannabinoid and immune systems: a potential dysregulation in depression? Psychopharmacology (Berl) 233, 1591–1604. https://doi.org/10.1007/s00213-015-4105-9.

Borgi, M., Collacchi, B., Ortona, E., et al., 2020. Stress and coping in women with breast cancer:unravelling the mechanisms to improve resilience. Neurosci. Biobehav. Rev. 119, 406–421. https://doi.org/10.1016/j.neubiorev.2020.10.011.

Calderón, L., Boehm, T., 2012. Synergistic, context-dependent, and hierarchical functions of epithelial components in thymic microenvironments. Cell 149, 159–172. https://doi.org/10.1016/j.cell.2012.01.049.

Chirico, A., Maiorano, P., Indovina, P., et al., 2020. Virtual reality and music therapy as distraction interventions to alleviate anxiety and improve mood states in breast cancer patients during chemotherapy. J. Cell. Physiol. 235, 5353–5362. https://doi.org/10.1002/jcp.29422.

Corren, J., Ziegler, S.F., 2019. TSLP: from allergy to cancer. Nat. Immunol. 20, 1603–1609. https://doi.org/10.1038/s41590-019-0524-9.

Cruceriu, D., Baldasici, O., Balacescu, O., et al., 2020. The dual role of tumor necrosis factor-alpha (TNF-α) in breast cancer: molecular insights and therapeutic approaches. Cell. Oncol. 43, 1–18. https://doi.org/10.1007/s13402-019-00489-1.

Dell'Osso, L., Carmassi, C., Mucci, F., et al., 2016. Depression, Serotonin and tryptophan. Curr. Pharmaceut. Des. 22, 949–954. https://doi.org/10.2174/1381612822666151214104826.

Dong, X.-Z., Li, Z.-L., Zheng, X.-L., et al., 2013. A representative prescription for emotional disease, Ding-Zhi-Xiao-Wan restores 5-HT system deficit through interfering the synthesis and transshipment in chronic mild stress-induced depressive rats. J. Ethnopharmacol. 150, 1053–1061. https://doi.org/10.1016/j.jep.2013.10.018.

Douglass, S., Ali, S., Meeson, A.P., et al., 2012. The role of FOXP3 in the development and metastatic spread of breast cancer. Cancer Metastasis Rev. 31, 843–854. https://doi.org/10.1007/s10555-012-9395-3.

Fraga, C.H., True, L.D., Kirk, D., 1998. Enhanced expression of the mesenchymal marker, vimentin, in hyperplastic versus normal human prostatic epithelium. J. Urol. 159, 270–274. https://doi.org/10.1016/s0022-5347(01)64080-1.

Gao, G.S., Li, Y., Zhai, H., et al., 2017. Humanin analogue, S14G-humanin, has neuroprotective effects against oxygen glucose deprivation/reoxygenation by reactivating Jak2/Stat3 signaling through the PI3K/AKT pathway. Exp. Ther. Med. 14, 3926–3934. https://doi.org/10.3892/etm.2017.4934.

Gennery, A.R., 2018. Predicting the future with TRECs. Blood 132, 1731–1733. https://doi.org/10.1182/blood-2018-09-873638.

Gloushankova, N.A., Zhitnyak, I.Y., Rubtsova, S.N., 2018. Role of epithelial-mesenchymal transition in tumor progression. Biochemistry (Mosc.) 83, 1469–1476. https://doi.org/10.1134/s0006297918120052.

Greenlee, H., DuPont-Reyes, M.J., Balneaves, L.G., et al., 2017. Clinical practice guidelines on the evidence-based use of integrative therapies during and after breast cancer treatment. CA Cancer J Clin 67, 194–232. https://doi.org/10.3322/caac.21397.

Hajj, A., Hachem, R., Khoury, R., et al., 2021. Clinical and genetic factors associated with anxiety and depression in breast cancer patients: a cross-sectional study. BMC Cancer 21, 872. https://doi.org/10.1186/s12885-021-08615-9.

Harrath, A.H., Jalouli, M., Oueslati, M.H., et al., 2021. The flavonoid, kaempferol-3-O-apiofuranosyl-7-O-rhamnopyranosyl, as a potential therapeutic agent for breast cancer with a promoting effect on ovarian function. Phytother Res. 35, 6170–6180. https://doi.org/10.1002/ptr.7067.

He, B.Q., Shi, R.Z., Luo, Q.H., et al., 2021. Ruyong Formula (RYF) Attenuates the Abnormal Phenotypic Changes of Thymic Epithelial Cells in 4T1 Breast Cancer Mice. https://doi.org/10.21203/rs.3.rs-591139/v1 preprint.

Huang, S.M., Chien, L.Y., Tai, C.J., et al., 2013. Effectiveness of 3-week intervention of Shi Quan Da Bu Tang for alleviating hematotoxicity among patients with breast carcinoma receiving chemotherapy. Integr. Cancer Ther. 12, 136–144. https://doi.org/10.1177/1534735412450513.

Jo, K., Santos-Buitrago, B., Kim, M., et al., 2020. Logic-based analysis of gene expression data predicts association between TNF, TGFB1 and EGF pathways in basal-like breast cancer. Methods 179, 89–100. https://doi.org/10.1016/j.ymeth.2020.05.008.

Kaplanov, I., Carmi, Y., Kornetsky, R., et al., 2019. Blocking IL-1β reverses the immunosuppression in mouse breast cancer and synergizes with anti-PD-1 for tumor abrogation. Proc. Natl. Acad. Sci. U.S.A. 116, 1361–1369. https://doi.org/10.1073/pnas.1812266115.

Ke, F., Wang, Z., Song, X., et al., 2017. Cryptotanshinone induces cell cycle arrest and apoptosis through the JAK2/STAT3 and PI3K/Akt/NFκB pathways in cholangiocarcinoma cells. Drug Des. Dev. Ther. 11, 1753–1766. https://doi.org/10.2147/dddt.S132488.

Lee, J., Jung, J.H., Kim, W.W., et al., 2021. Short-term serial assessment of electronic patient-reported outcome for depression and anxiety in breast Cancer. BMC Cancer 21, 1065. https://doi.org/10.1186/s12885-021-08771-y.

Lim, J.A., Oh, C.S., Yoon, T.G., et al., 2018. The effect of propofol and sevoflurane on cancer cell, natural killer cell, and cytotoxic T lymphocyte function in patients undergoing breast cancer surgery: an in vitro analysis. BMC Cancer 18, 159. https://doi.org/10.1186/s12885-018-4064-8.

Liu, S., Zhang, D., Wu, J., et al., 2019. Shenqi fuzheng injection in the treatment of breast cancer: a meta-analysis of randomized controlled trials. Integr. Cancer Ther. 18, 1534735418816824 https://doi.org/10.1177/1534735418816824.

Lopes, C., Lopes-Conceição, L., Fontes, F., et al., 2022. Prevalence and persistence of anxiety and depression over five years since breast cancer diagnosis-the NEON-BC prospective study. Curr. Oncol. 29, 2141–2153. https://doi.org/10.3390/curroncol29030173.

Lu, Y., Zhou, J., Xu, C., et al., 2008. JAK/STAT and PI3K/AKT pathways form a mutual transactivation loop and afford resistance to oxidative stress-induced apoptosis in cardiomyocytes. Cell. Physiol. Biochem. 21, 305–314. https://doi.org/10.1159/000129389.

Ma, W., Liu, P., Zheng, J., et al., 2021. Immune and nonimmune mechanisms mediate the mental stress-induced tumor growth in a xenograft model of breast cancer. Cell Death Dis. 12, 987. https://doi.org/10.1038/s41419-021-04280-9.

Ma, Y., Ren, Y., Dai, Z.J., et al., 2017. IL-6, IL-8 and TNF-α levels correlate with disease stage in breast cancer patients. Adv. Clin. Exp. Med. 26, 421–426. https://doi.org/10.17219/acem/62120.

Marković, I., Savvides, S.N., 2020. Modulation of signaling mediated by TSLP and IL-7 in inflammation, autoimmune diseases, and cancer. Front. Immunol. 11, 1557. https://doi.org/10.3389/fimmu.2020.01557.

Medici, D., Hay, E.D., Goodenough, D.A., 2006. Cooperation between snail and LEF-1 transcription factors is essential for TGF-beta1-induced epithelial-mesenchymal transition. Mol. Biol. Cell 17, 1871–1879. https://doi.org/10.1091/mbc.e05-08-0767.

Mohammad, M.G., Raftos, D.A., Joss, J., 2009. Cytoskeletal proteins in thymic epithelial cells of the Australian lungfish Neoceratodus forsteri. J. Anat. 214, 140–152. https://doi.org/10.1111/j.1469-7580.2008.00995.x.

Nitta, T., Suzuki, H., 2016. Thymic stromal cell subsets for T cell development. Cell. Mol. Life Sci. 73, 1021–1037. https://doi.org/10.1007/s00018-015-2107-8.

Nobrega, C., Nunes-Alves, C., Cerqueira-Rodrigues, B., et al., 2013. T cells home to the thymus and control infection. J. Immunol. 190, 1646–1658. https://doi.org/10.4049/jimmunol.1202412.

O'Rourke, K.P., Dow, L.E., Lowe, S.W., 2016. Immunofluorescent staining of mouse intestinal stem cells. Bio Protoc 6. https://doi.org/10.21769/bioprotoc.1732.

Pattarini, L., Trichot, C., Bogiatzi, S., et al., 2017. TSLP-activated dendritic cells induce human T follicular helper cell differentiation through OX40-ligand. J. Exp. Med. 214, 1529–1546. https://doi.org/10.1084/jem.20150402.

Peinado, H., Olmeda, D., Cano, A., 2007. Snail, Zeb and bHLH factors in tumour progression: an alliance against the epithelial phenotype? Nat. Rev. Cancer 7, 415–428. https://doi.org/10.1038/nrc2131.

Quentmeier, H., Drexler, H.G., Fleckenstein, D., et al., 2001. Cloning of human thymic stromal lymphopoietin (TSLP) and signaling mechanisms leading to proliferation. Leukemia 15, 1286–1292. https://doi.org/10.1038/sj.leu.2402175.

Ravkov, E., Slev, P., Heikal, N., 2017. Thymic output: assessment of CD4(+) recent thymic emigrants and T-Cell receptor excision circles in infants. Cytometry B Clin Cytom 92, 249–257. https://doi.org/10.1002/cyto.b.21341.

Roan, F., Bell, B.D., Stoklasek, T.A., et al., 2012. The multiple facets of thymic stromal lymphopoietin (TSLP) during allergic inflammation and beyond. J. Leukoc. Biol. 91, 877–886. https://doi.org/10.1189/jlb.1211622.

Schindler, C., Levy, D.E., Decker, T., 2007. JAK-STAT signaling: from interferons to cytokines. J. Biol. Chem. 282, 20059–20063. https://doi.org/10.1074/jbc.R700016200.

Shen, J.M., Ma, L., He, K., et al., 2020. Identification and functional study of immortalized mouse thymic epithelial cells. Biochem. Biophys. Res. Commun. 525, 440–446. https://doi.org/10.1016/j.bbrc.2020.02.083.

Siersbæk, R., Scabia, V., Nagarajan, S., et al., 2020. IL6/STAT3 signaling hijacks estrogen receptor α enhancers to drive breast cancer metastasis. Cancer Cell 38, 412–423. e419. https://doi.org/10.1016/j.ccell.2020.06.007.

Tang, M., Chen, M., Li, Q., 2021. Paeoniflorin ameliorates chronic stress-induced depression-like behavior in mice model by affecting ERK1/2 pathway. Bioengineered 12, 11329–11341. https://doi.org/10.1080/21655979.2021.2003676.

Wohlmann, A., Sebastian, K., Borowski, A., et al., 2010. Signal transduction by the atopy-associated human thymic stromal lymphopoietin (TSLP) receptor depends on Janus kinase function. Biol. Chem. 391, 181–186. https://doi.org/10.1515/bc.2010.029.

Wu, Y., Zhang, Y., Wu, J.A., et al., 1998. Effects of Erkang, a modified formulation of Chinese folk medicine Shi-Quan-Da-Bu-Tang, on mice. J. Ethnopharmacol. 61, 153–159. https://doi.org/10.1016/s0378-8741(98)00027-0.

Wu, Y.J., Wong, B.S., Yea, S.H., et al., 2016. Sinularin induces apoptosis through mitochondria dysfunction and inactivation of the pI3K/Akt/mTOR pathway in gastric carcinoma cells. Mar. Drugs 14. https://doi.org/10.3390/md14080142.

Xie, F., Sun, Y.J., Zhang, D.X., et al., 2017. 100 Cases of non-lactating mastitis treated with ruyong formula and external application. World Journal of Integrated Traditional and Western Medicine 12, 372–373+421. https://doi.org/10.13935/j.cnki.sjzx.170320.

Yamanaka, Y., Nakajima, K., Fukada, T., et al., 1996. Differentiation and growth arrest signals are generated through the cytoplasmic region of gp130 that is essential for Stat3 activation. EMBO J. 15, 1557–1565.

Yang, X.O., Panopoulos, A.D., Nurieva, R., et al., 2007. STAT3 regulates cytokine-mediated generation of inflammatory helper T cells. J. Biol. Chem. 282, 9358–9363. https://doi.org/10.1074/jbc.C600321200.

Yu, S., Li, W., Tang, L., et al., 2022. Depression in breast cancer patients: immunopathogenesis and immunotherapy. Cancer Lett. 536, 215648 https://doi.org/10.1016/j.canlet.2022.215648.

Zhang, M., Zhou, L., Xu, Y., et al., 2020. A STAT3 palmitoylation cycle promotes T(H)17 differentiation and colitis. Nature 586, 434–439. https://doi.org/10.1038/s41586-020-2799-2.

Zhang, S., Lu, Y., Chen, W., et al., 2021. Network pharmacology and experimental evidence: PI3K/AKT signaling pathway is involved in the antidepressive roles of chaihu shugan san. Drug Des. Dev. Ther. 15, 3425–3441. https://doi.org/10.2147/dddt.S315060.

Zhou, F., Li, Y.H., Wang, J.J., et al., 2017. Endoplasmic reticulum stress could induce autophagy and apoptosis and enhance chemotherapy sensitivity in human esophageal cancer EC9706 cells by mediating PI3K/Akt/mTOR signaling pathway. Tumour Biol 39, 1010428317705748. https://doi.org/10.1177/1010428317705748.

Zhu, Z.H., 2005. Danxi's Experiential Therapy, vol. 5. People's Medical Publishing House Beijing.